CFD Investigation of the Effects of Split Main Fuel Injection Parameters on Combustion and Emissions in a Light-Duty Diesel Engine

H.K. Ng
The School of Mechanical Engineering
The University of Nottingham Malaysia Campus
Jalan Broga, 43500 Semenyih
Selangor, Malaysia
hoonkiat.ng@nottingham.edu.my

P.J. Shayler
The School of Mechanical, Materials and Manufacturing Engineering
The University of Nottingham
University Park, Nottingham NG7 2RD, United Kingdom
paul.shayler@nottingham.ac.uk

Abstract: The paper outlines CFD investigations on the combustion and emission effects of the fuel injection strategies in a direct injection diesel engine fitted with a high pressure common rail fuel injection system. Strategies using a split main injection has been explored, with the variables of interest including the ratio of the first to second part of the main, the separation between these and the timing of the start of main injection. Exhaust gas recirculation rate was a fourth variable. The main influence of these 4 parameters on the nature of the combustion, and the resulting NO and soot emissions is characterised. Model validation has been based on comparisons with experimental data for heat release rate and engine-out emissions values. Simulations have been performed under typical part-load operating conditions, where the temporal and spatial developments of combustion/emissions processes are mapped out.

Keywords: CFD, Injection, Combustion, NO_x and Soot.

1.   Introduction

The superior fuel economy and durability of direct injection diesel engines have made these an attractive alternative to gasoline engines for passenger cars and light commercial vehicles. The market share of diesel-powered vehicles continues to rise, especially in Europe [1], and the continuing evolution of diesel technology remains a promising route to meeting future requirements for fuel efficiency and emissions control [2]. However, on the debit side, untreated emissions of NO_x and particulates from diesel engines make a significant contribution to levels of these pollutants in the atmosphere. Engine-out exhaust gas concentrations of NO_x, which comprises of nitric oxide and nitrogen dioxide, are similar to those of gasoline engines, and around 0.2 to 0.5% of the fuel mass is emitted as small (~0.1µm diameter) particulates [3] consisting predominantly of carbonaceous soot with absorbed organic hydrocarbons. The emissions are perceived to pose serious threats to public health and the environment, including increased exposure to carcinogens, cardiovascular/respiratory problems, visibility reduction, adverse changes to global climate and water/soil contamination. The large increases in vehicle population and vehicle miles travelled (VMT) in rapidly developing countries in Asia, the Indian Sub Continent and elsewhere can only add to the problems caused by an ageing fleet of diesel-powered public and commercial transportations using archaic diesel technology. In numerous large Asian cities, concentrations of noxious substances along traffic thoroughfares and adjacent locales where people live and work already exceed allowable limits and standards set by those countries [4].

Global efforts to limit diesel emissions are characterised by increasingly stringent regulations in many areas of the world. Since the revised European Council emissions directive (Euro I) was enforced in 1991, there has been a significant reduction in tailpipe emission levels at every stage, culminating in the present Euro IV emissions standard. Comparable efforts are also taken by the US Environmental Protection Agency (EPA). Although high levels of exhaust gas recirculation (EGR), fuel reformulation and aftertreatment devices such as lean NO_x catalysts and particulate filters have made considerable inroads to reducing NO_x and soot in the exhaust stream, the emissions standards for Euro V and beyond require further improvement still but in a cost-effective manner [1,5]. One of these techniques lies in recent advancement in the high pressure common rail (HPCR) fuel injection system for light duty automotive diesel engines. The enhanced flexibility and control over fuel injection pattern to achieve particular potential benefits are made possible by fast-acting solenoid or piezo-electric injectors, coupled with high pressure fuel reservoir in the rail [6]. There is

considerable interest in determining how the flexibility of fuel injection offered by the HPCR system might contribute to the reduction in NO_x and particulates emissions, while maintaining its fuel economy superiority. The precise and adaptable fuel delivery of an HPCR system allows up to six separate pulses within the engine cycle. With multiple injection strategies, optimisation of the fuel injection pattern across the engine operating map is a difficult task, particularly when other parameters such as exhaust gas recirculation level and turbocharger boost pressure may also be treated as independent calibration values. Interactions between these can give rise to non-linear trends to combustion and emissions characteristics. To that end, detailed understanding of the effects of injection parameters on diesel spray combustion and emissions formation is essential, and the work reported here is concerned with the use of CFD simulation to achieve this.

There are now several well-established codes available as commercial products, and others have been developed by OEMs for in-house use. For one or more reasons, which include high licence costs, restrictions on access to source codes and hardware requirements, these are not exploited in the study here. Instead, KIVA-3V Release 2 has been used to explore spatial and temporal distributions of NO and soot during the engine cycle. This simulation study was undertaken to complement experimental studies on a single-cylinder 0.5l engine fitted with modern HPCR system. The main parameters of interest were the ratio of the first to second contributions to the main injection event, defined as a mass ratio, and the separation between these. The separation is defined as the crank angle degrees of separation between the end of the first injection and the start of the second. The start of the main injection (SOI) and exhaust gas recirculation (EGR) were changed only to examine how the effects of split main ratio and separation were modified. Influences on NO_x and soot were of chief interest. The results presented are for a fixed engine speed of 1600 rev/min and BMEP of 6.76 bar.

2.   Formulation and Evaluation of Numerical Models

KIVA-3V Release 2 has been used with modifications which enable the code to be implemented on PCs using the Linux operating system [1,7]. The combustion system was of bowl-in-piston and flat cylinder head face configuration, with fuel injection provided by a six-hole injector installed vertically and centrally. The compression ratio for the combustion system is 18.2:1 and has a swept volume of 500 cc. In all cases, rail pressures were fixed at around 850 bar, and the main fuel delivery is preceded by a pilot injection with the quantity of 2.9 mg per cycle.

For the simulation studies, a 60° sector mesh was adopted to represent one-sixth of the combustion chamber by assuming the chamber's symmetry consistent with the six-hole injector. This allows significant reduction in computational runtime and demands for computational resources, but imposes a periodicity of the velocity field on solutions and any spray-spray interactions would have to be neglected. The squish volume was adjusted to account for the absence of a crevice submodel and match the compression ratio of the experimental engine [8,9]. Only the closed portion of cycle, from inlet valve closing to exhaust valve opening, is simulated. For all the results presented, conditions in the cylinder at the time of inlet valve closure (IVC) were matched to intake manifold conditions. Pressure and temperature were set to   1 bar and 313 K, respectively. $C_{12}H_{26}$ was selected as the fuel model to represent the light diesel fuel used [10,11,12], and the spray was defined as having a cone angle of 25°, an initial temperature of 285 K and a SMR of 70 µm. The injection rate profiles were matched to the recorded volumetric flow rate of the injector at different pulse width at specified rail pressure values.

No modifications have been made to the fundamentals of the submodels in the standard code. There is, however, considerable freedom to adjust values of initial/boundary inputs and coefficients for a given application. Here, adjustments were made solely to match experimental data for pressure and heat release traces, and exhaust engine-out emissions values. The same coefficient settings were then used for all the simulations. Apart from NO and soot models described below, the submodels used for the study are summarised in Table 1. Three mesh configurations were used to investigate the effects of mesh resolution on computational accuracy. The sector mesh with 28,389 cells is found to give adequately grid independent results, where reasonable trade-off between computing resources and accuracy is achieved. This has 32 cells in the radial direction, 30 cells in the azimuthal direction and 30 cells in the axial direction at BDC. Typical grid size is approximately 1.24 mm in the axial direction and 1.44 mm in the radial direction within the piston bowl, with the azimuthal grid spacing at 2.0^o. The simulation runtime using this mesh configuration over the closed part of the cycle for this test engine was typically around 4.5 hours.

Table 1: Submodels used for the simulations.

	Submodels of KIVA-3V Release II
Intake flow	Assumed initial in-cylinder flow
Combustion	• Arrhenius (at auto-ignition point) [11,13] • Mixing-controlled turbulent combustion [14,15]
Heat transfer	Modified law-of-the-wall [14,16]
Fuel model	$C_{12}H_{26}$ [10,11,12]
Wall film dynamics	Particle-based with splash models [14,17]
Dynamics of evaporating spray	Monte Carlo-based discrete particle technique [18,19]
Turbulence model	Modified RNG κ - ε [14,20]
Fuel vaporisation	Single component
Drop breakup/distortion/oscillation	Taylor Analogy Breakup model [18,21]
Drop drag	Distorting spherical drop [22,23]

During diesel combustion, most in-cylinder NO_x is in the form of NO [24], and NO_2 is produced from the rapid conversion of NO [25,26]. Therefore, NO is commonly perceived as the precursor of all NO_x species measured in tailpipe emission, and it is deemed sufficient to only consider NO in the modeling work. Thermal NO formation in the bulk-gas postflame mixture usually accounts for the dominant source of NO under diesel combustion environment. The contributions of mechanisms such as N_2O intermediate, prompt NO (Fenimore-NO) and fuel nitrogen have not been represented. Thermal NO formation can be adequately described by the extended Zel'dovich NO mechanism [3,27]:

$$O + N_2 \underset{k_{1b}}{\overset{k_{1f}}{\rightleftharpoons}} N + NO \tag{1}$$

$$O_2 + N \underset{k_{2b}}{\overset{k_{2f}}{\rightleftharpoons}} O + NO \tag{2}$$

$$N + OH \underset{k_{3b}}{\overset{k_{3f}}{\rightleftharpoons}} H + NO \tag{3}$$

The rate constants of the Arrhenius form used are given in Table 2. These are based on values recommended by Bowman [28]. Finally, to match the experimental engineout NO_x data, the simulation results for NO were multiplied by a constant factor of 1.46. The need for the multiplier is attributed to the neglect of other mechanisms of NO_x formation at high pressure [29,30] and to the underestimation of thermal NO formation given by the extended Zel'dovich mechanism.

Table 2: Rate constants for the extended Zel'dovich NO formation mechanism.

Rate constants for NO formation mechanism in cm^3/(mol . s)	
k_{1f}	$1.4 \times 10^{14}\, e^{\frac{-38,000}{T}}$
k_{1b}	1.6×10^{13}
k_{2f}	$6.4 \times 10^9\, T\, e^{\frac{-3,150}{T}}$
k_{2b}	$1.5 \times 10^9\, T\, e^{\frac{-19,500}{T}}$
k_{3f}	4.0×10^{13}
k_{3b}	$2.0 \times 10^{14}\, e^{\frac{-23,650}{T}}$

In applications to diesel engines, it is common to describe the rate of change of soot mass per unit volume (M_s) as the difference between rates of formation and destruction,

$$\frac{dM_s}{dt} = \frac{dM_{sf}}{dt} - \frac{dM_{so}}{dt}$$

(4)

where M_{sf} is the mass of soot formed and M_{so} as the mass of soot oxidised.

The soot formation model in KIVA-3V is based on the mathematical descriptions first developed by Surovikin [31,32]. The formation model comprises of radical nuclei formation, follow by the intermediate step of radical nuclei growth and finally the inception of physical soot particles. Modified parameters from those proposed by Surovikin were used, as presented in Table 3.

Table 3:   Modified input parameters for the soot formation model.

Input parameters	Values
Activation energy for radical nuclei formation	$141.0 \ \frac{kcal}{mol}$
Activation energy for radical nuclei growth	$33.0 \ \frac{kcal}{mol}$
Activation energy for particle nuclei growth	$12.0 \ \frac{kcal}{mol}$
Activation energy of radical nuclei and soot interaction	$0.0 \ \frac{kcal}{mol}$
Number of carbon atoms per hydrocarbon molecule	12
Minimum radius of HC molecule	$2.0 \times 10^{-8} \ cm$
Particle nuclei density	$2.5 \ \frac{g}{cm^3}$
Critical diameter of radical nuclei	$8.5 \times 10^{-8} \ cm$
Initial diameter of the growing radical nuclei	$3.5 \times 10^{-8} \ cm$

Soot burn out is generally believed to take place predominantly in oxygen-containing regions beyond the soot formation site [3], although O, OH, H_2O, CO_2, NO, N_2O and NO_2 are also possible sources of oxidants [33,34,35]. The oxygen soot reduction mechanism adopted by KIVA-3V adhered to the procedures by Haynes and Wagner [36], with the semi-empirical oxidation rate constants based on the values proposed by Nagle and Strickland-Constable [37,38]. The model assumes that there are two types of reaction sites on the carbon surface available for oxygen attack, with one considerably more reactive than the other [14]. For the more reactive sites, the rate is controlled by the fraction of sites not covered by surface oxides, whereas in the less reactive sites, the reaction rate has a first order dependence on oxygen concentration [36,37,38]. The rate constants for the reactions are shown in Table 4. With the parameter values given in Tables 4 and 5, predicted soot mass in the exhaust gas stream (as a fraction of the total fuel injected) were in good agreement with the measured values. These were derived from the Filter Smoke Numbers (FSN) given by an AVL 415S Variable Sampling Smoke Meter instrument [39,40,41].

Table 4: Rate constants for Nagle and Strickland-Constable soot oxidation mechanism.

Rate constants	Units
$k_A = 20\ e^{\frac{-30,000}{RT}}$	$g/cm^2 \cdot s \cdot atm$
$k_B = 4.46 \times 10^{-3}\ e^{\frac{-15,200}{RT}}$	$g/cm^2 \cdot s \cdot atm$
$k_T = 6.31 \times 10^4\ e^{\frac{-97,000}{RT}}$	$g/cm^2 \cdot s$
$k_Z = 21.3\ e^{\frac{+4,100}{RT}}$	atm^{-1}

3. Results

When one of the four factors is explored in the computational study, the others were held constant at their respective nominal settings. The results presented here are representative of the ranges investigated. Here we have concentrated on the effects of soot and NO_x variation. Whenever information on species spatial distributions is required, 2D contour plots are made on sliced vertical planes along the spray axis. This is to provide a 3D perspective representation of the combustion chamber near the spray without the confusions that may arise from overlapped and hidden details of a full 3D plot.

Results for a single injection case have been included as a reference for comparison in the following simulation results. There are significant differences between the single injection case and the case of a split main injection with zero separation. The latter includes the closing of the injector needle between the first and second part of the split main, producing a perturbation in the rate of fuel injection.

Effect of Split Main Ratio when Separation is Small

This first set of simulation results illustrates the influence of split main ratio with zero separation, for a fixed start of injection of -6° ATDC and zero exhaust gas re-circulation rate. The temporal variations of net in-cylinder soot mass are shown in Figure 1(a). Significant amount of soot appears at -2° ATDC, with similar rate of soot mass increment for each of the three injection profiles. Peak soot mass contents are reached around 2° after the end of the first injection pulse, and this values increase in the order of increasing ratio. Thereafter, soot falls at a similar rate and the order set by the peak values follows through to the engine-out levels. From the temporal soot mass variation, there are no major features to identify with the second injection. By inspection of Figure 1(b), second injection event produces very limited secondary soot cloud, and has little interaction with the soot mass associated with the first pulse. From Figure 2, secondary soot formation is seized because the short dwell period preceding the start of second injection provided an ideal environment for the second spray jet to be leaner. Thus, peak and exhaust soot levels are only determined by the amount of soot formed due to the first injection pulse. The effect of split main ratio on soot distribution is also illustrated in Figure 1(b). As ratio increases, the concentration within the soot cloud is raised, but it is still distributed along the side of the bowl through the bowl lip into parts of the squish region. CFD results suggest this is primarily caused by an increase in soot production from the less complete combustion of locally richer first spray jet when the split main ratio is higher.

Cumulative NO variation in Figure 3(a) shows that the lowest engine-out NO is produced by the single injection profile, and the highest by the lowest split main ratio. In all cases, NO concentration is saturated by 25° ATDC. From knowledge of previous studies [1,42], gas mass fraction with a temperature above 2650 K provides a good indication of NO productions in and around of combustion zones. The order of highest to lowest for NO concentration is reflected in Figure 3(b), where the lower split main ratios give slightly higher mass fraction of high-temperature gas. From the in-cylinder temperature and NO distributions illustrated in Figure 4, highest NO concentration is consistently located in regions of high temperature post-combustion gas. Visual examination on the contour plots show that the single injection case gives the lowest final NO concentration because the local gas temperature is considerably lower than for the other cases. With high split main ratio, most of the NO is confined to the inside of the bowl. As the ratio is lowered, slightly increased fraction of the post-combustion gas is moved into the squish region, which displaces regions with high NO concentration into the outer part of the combustion chamber.
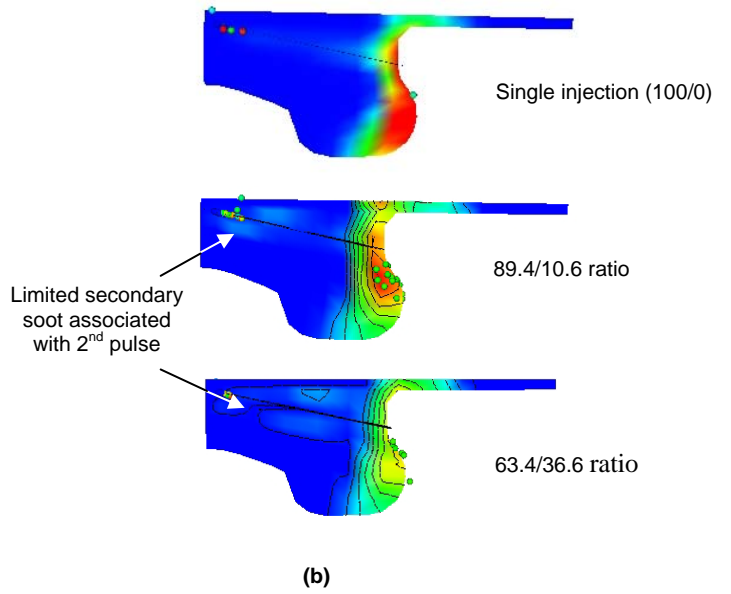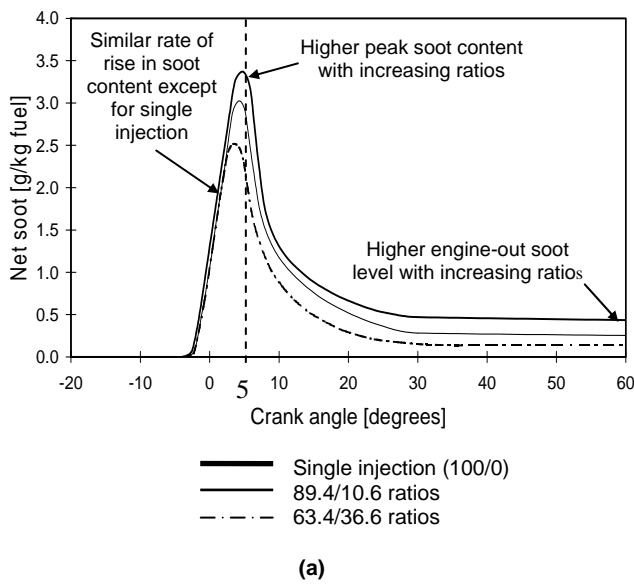
Fig 1: Effects of split main ratios at fixed –6.0° ATDC main SOI and 0.0° separation on the amount of in-cylinder net soot content (a), and the associated 2D soot mass contour plots at 5.0° ATDC (b).
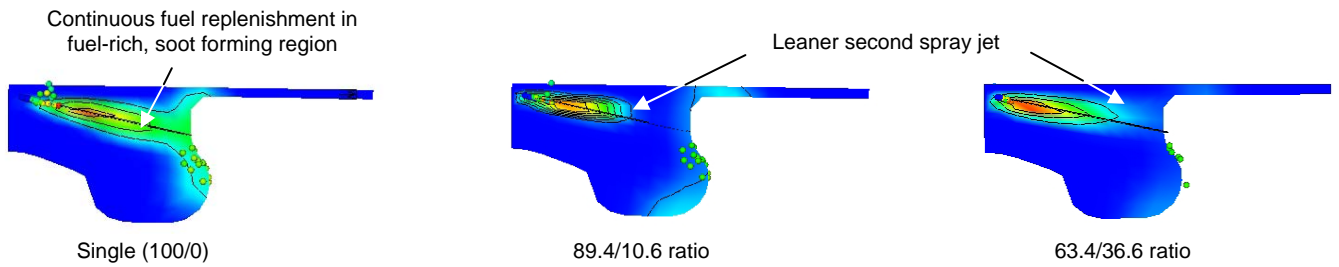

Fig 2: Distribution of diesel fuel vapour at 1.0° after the onset of second injection event (except for single injection case)
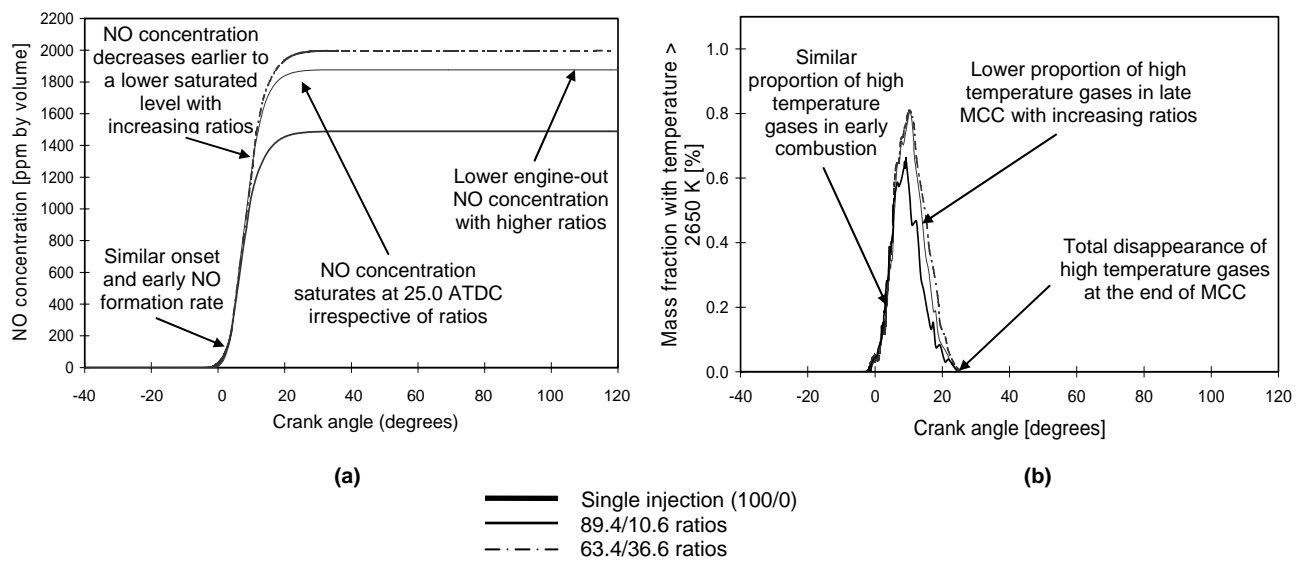

Fig 3: Effects of split main ratios at fixed –6.0° ATDC main SOI and 0.0° separation on

(a) time evolution of in-cylinder NO concentrations,
(b) time variation of the proportion of gas mass fraction with temperature > 2650 K.

(a)

(b)

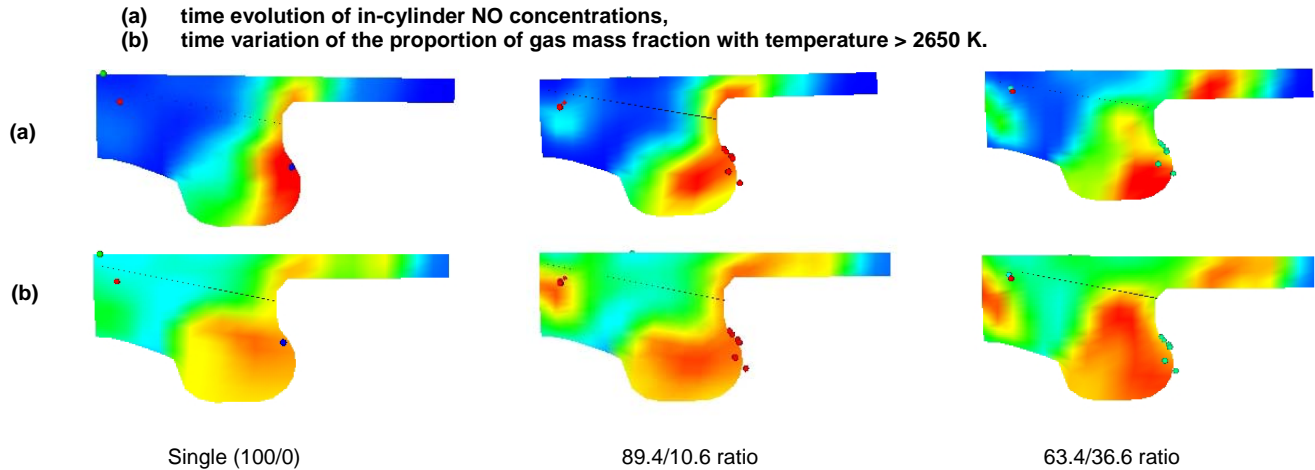Single (100/0)   89.4/10.6 ratio   63.4/36.6 ratio

Fig 4: Spatial distribution at 15.0° ATDC, for split main ratio at fixed –6.0° ATDC main SOI and 0.0° separation:
(a,upper): NO concentrations,
(b,lower): temperature field.

Effect of Split Main Ratio when Separation is Large

The variations of soot mass fraction for two split main ratio cases with a separation of 20°, together with a baseline single injection case are shown in Figure 5(a). As with the closed-coupled cases, peak soot values reflect the constraint on soot production associated with the first injection. However, this order is reversed during the mixing control combustion of the first injection because high temperature field experienced in cases with larger ratio accelerates the rate of soot reduction (Figure 5(b)). This culminates in the lowest ratio giving the highest soot levels prior to the start of the second injection. The higher temperature observed is a result of increasing heat release rate when fuel mass injected in the first pulse is raised for cases with higher ratio. The trend follows through during the second injection, until the exhaust valves opening time. The soot production and oxidation related to the second injection largely mimic that of the first. The increased fuel mass in the second injection when the ratio is low raises the fuel vapour concentration in the combusting jet core, leading to the rise in the secondary soot mass formed as illustrated in Figure 6(a-b). There is a mixed effect of the split main ratio on soot distribution. The influence of ratio is rather weak on the primary soot cloud, which is mostly located inside the bowl. In contrast, the location of secondary soot is greatly affected by ratio. Secondary soot impingement on the bowl lip with further penetration into the squish region occurs when the ratio is low. For cases with higher ratio, secondary soot is confined mainly to within the central region of the chamber.
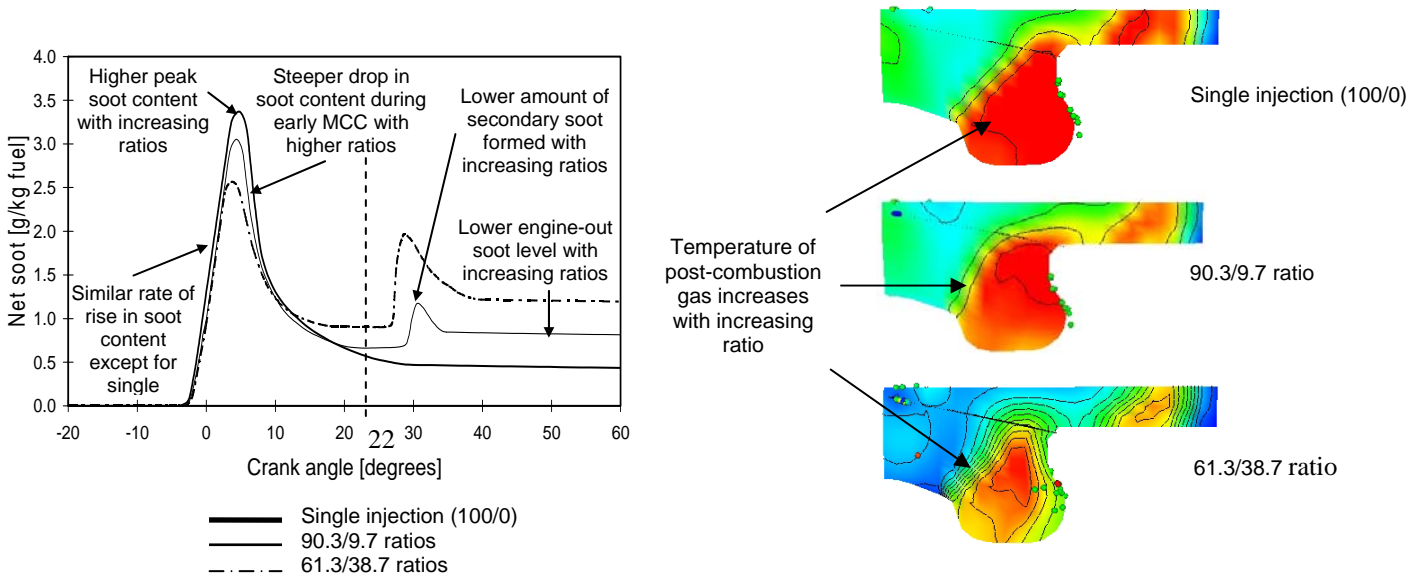

Single injection (100/0)

90.3/9.7 ratio

61.3/38.7 ratio

Fig 5: Effects of split main ratios at fixed –6.0° ATDC main SOI and 20.0° separation on the amount of in-cylinder net soot content (a), and the corresponding in-cylinder temperature field at 22.0° ATDC (b).
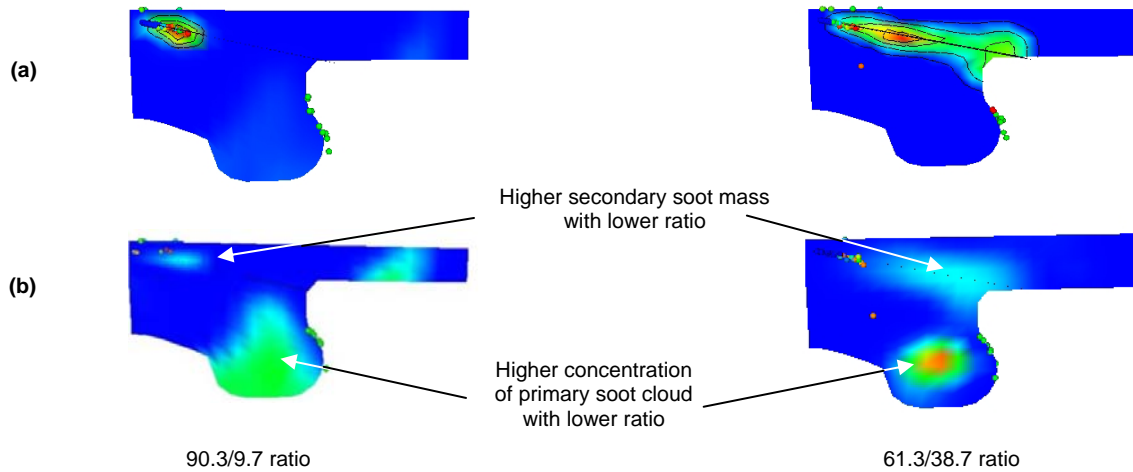

(a)

(b)

Higher secondary soot mass with lower ratio

Higher concentration of primary soot cloud with lower ratio

90.3/9.7 ratio

61.3/38.7 ratio

Fig 6: Spatial distribution at 28.0° ATDC, for split main ratio at fixed –6.0° ATDC main SOI and 20.0° separation:
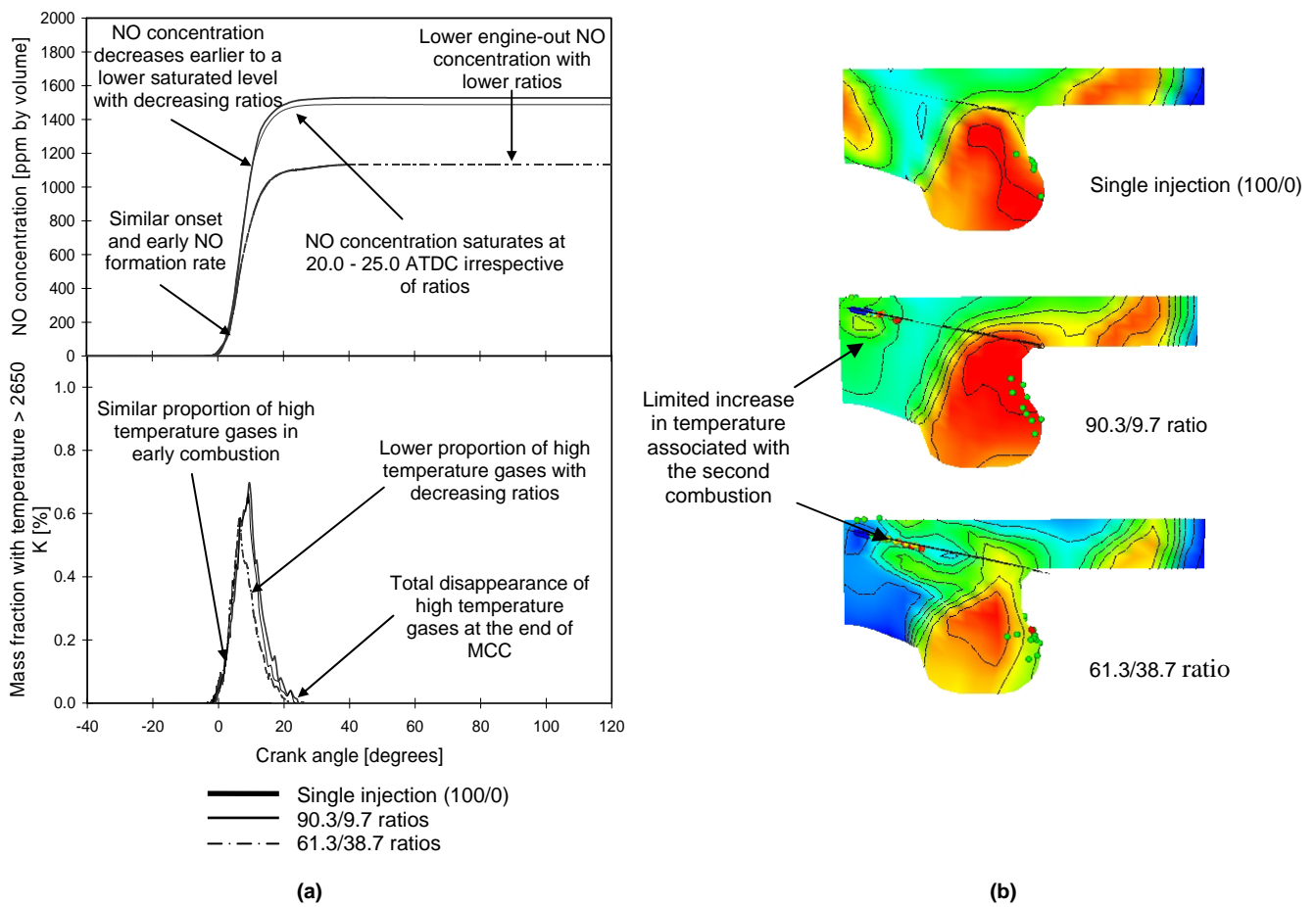(a,upper): fuel vapour,
(b,lower): soot mass.

NO concentration decreases earlier to a lower saturated level with decreasing ratios

Lower engine-out NO concentration with lower ratios

Similar onset and early NO formation rate

NO concentration saturates at 20.0 - 25.0 ATDC irrespective of ratios

Similar proportion of high temperature gases in early combustion

Lower proportion of high temperature gases with decreasing ratios

Total disappearance of high temperature gases at the end of MCC

Single injection (100/0)

90.3/9.7 ratio

61.3/38.7 ratio

Limited increase in temperature associated with the second combustion

Single injection (100/0)
90.3/9.7 ratios
61.3/38.7 ratios

(a)

(b)

Fig 7: Effects of split main ratios at fixed –6.0° ATDC main SOI and 20.0° separation on
(a): temporal variation of in-cylinder NO concentration and gas mass fraction with temperature > 2650 K,

The cumulative NO concentration curves in Figure 7(a) show the order of highest to lowest in-cylinder NO concentration is reversed by extending the separation from 0° to $20°$. Highest concentration of NO is seen in the single injection case, with the lowest concentration given by the lowest split main ratio. The high temperature gases associated with NO production exist only at crank angles earlier than $25°$ ATDC, indicating that the first pulse is all important in dictating the levels of NO. Observations made from Figure 7(b) confirm that the burning of the second pulse is insufficient to increase gas temperature to the level required to promote NO formation. As a result, there is no secondary NO sites unlike that of the soot. Thus, the fuel in the first injection is the dominant influence on NO production and the lower ratio gives the lowest proportion of mass at and above 2650K. The distribution of NO is not greatly modified by the split main ratio when the separation is large. In all cases, high concentration of NO is distributed mainly within the piston bowl, with a small proportion of this displaced into the squish region nearer to the cylinder wall.

Effect of Start of Injection (SOI timing)

In the SOI timing study, a swing of 8° was made from -6.0^o ATDC to 2.0^o ATDC. Advancing or retarding the start of the main injection timing has little influence on the shape of the soot and NO variations with time. However, retarding the SOI timing tends to raise the in-cylinder soot, but produces a decrease in NO concentration. The results presented here are based on a split main ratio of 63/37 with a 0.5^o separation, but they embodied the effects for the range of ratios and separations investigated. The fuel consumption penalty caused by retarding the SOI timing was given by the increase in the first injection period.

The temporal variations of soot mass for the close-coupled split main results are given in Figure 8(a). The small increase in the peak soot values by retarding the injection is carried through to give an approximate doubling in the engine-out soot levels. These higher soot levels are primarily due to the increment in soot formation because prolonged first injection associated with delayed SOI produces an increase fuel vapour concentration in the reacting spray jet. From the soot distribution plots in Figure 8(b), higher fraction of the primary soot cloud is distributed into the squish region as the SOI timing is moved further into the expansion stroke.

The effect of timing swing on NO is to halve the engine-out NO concentration, as shown in Figure 9(a). From the NO variations, delaying the SOI timing lowers the NO production rate, as well as shortening the production window because NO generation ceased at a similar crank angle of around 25.0^o ATDC. Delaying the main injection timing limits the global and local charge temperature required to promote NO generation. The higher NO concentration regions are predominantly confined within the piston bowl for advanced SOI timing, and delaying the injection will have the effect of distributing the lower NO concentration towards the side of the bowl (Figure 9(b)).
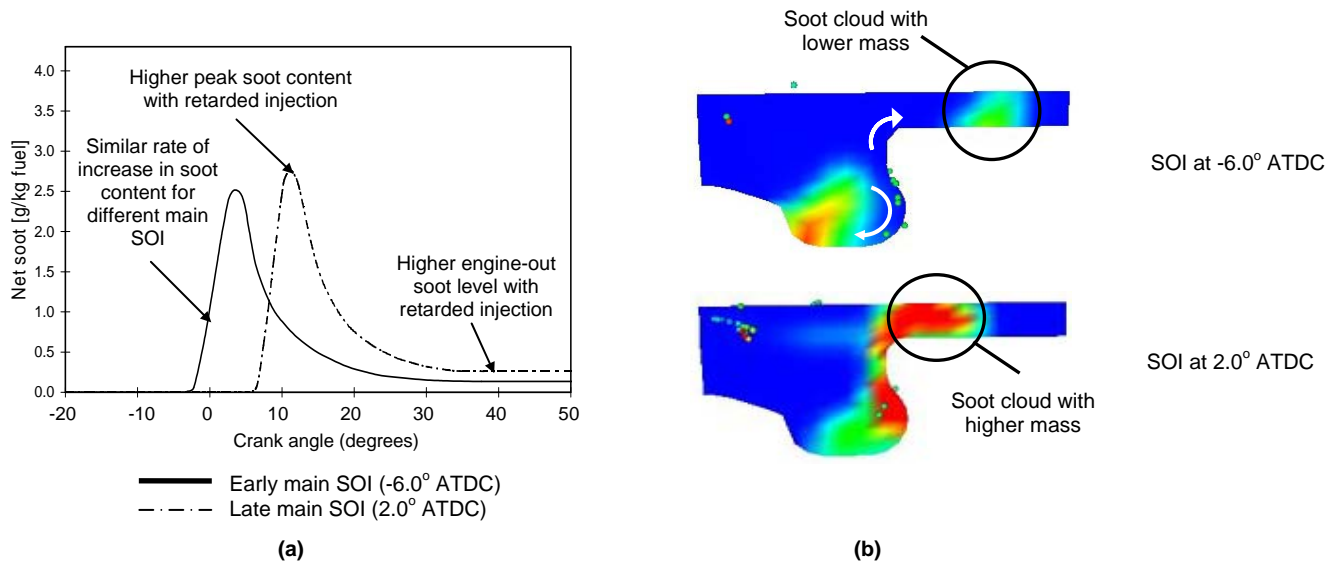

(a)   (b)

Fig 8:   Effects of main SOI under 63/37 ratio and at fixed 0.5^o separation conditions on
(a) in-cylinder net soot content,
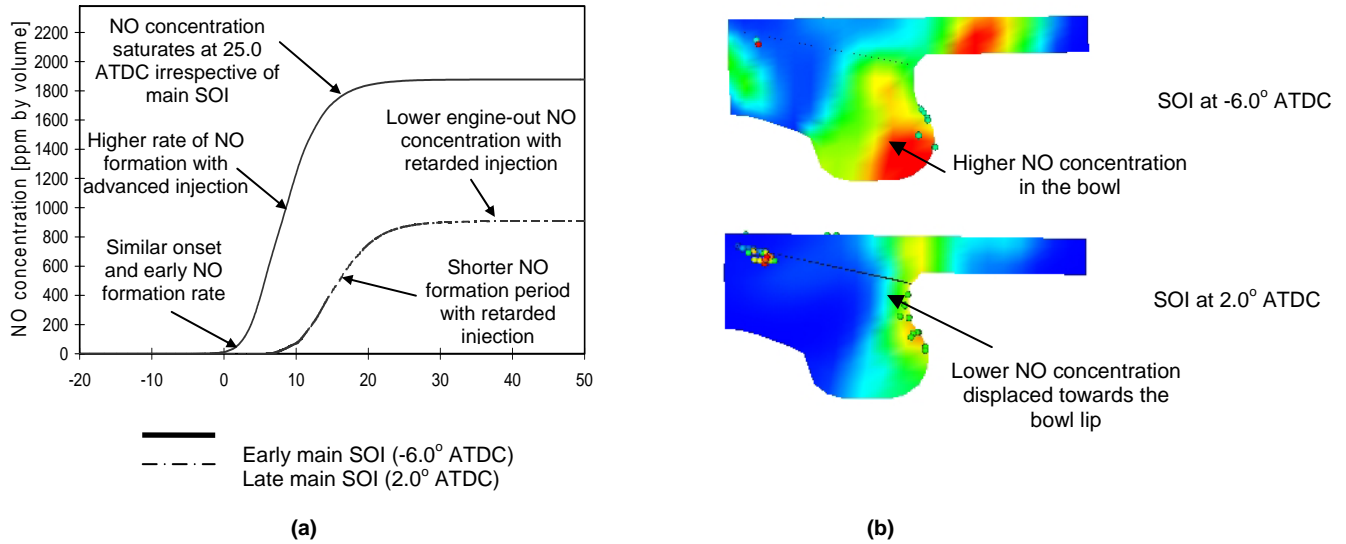**(b) spatial distribution of soot at 20.0^o ATDC.**

Fig 9: Effects of main SOI under 63/37 ratio and at fixed 0.5° separation conditions on
(a) in-cylinder NO concentration,
(b) spatial distribution of NO at 10.0° after the main SOI timing.

Effect of EGR

The results of introducing EGR on soot and NO profiles as a function of crank angles are illustrated for a close-coupled 60/40 ratio split main. The EGR effects discussed here are, however applicable throughout the values of ratio, separation and SOI timing investigated. With the introduction of a moderate level of 10.7% EGR, temporal variations of soot and NO have been scaled up or down without significant influence on the shape of the variations itself. The increase in the specific fuel consumption with EGR is indicated by an increase in the injection rate for both the first and second injection pulses.

Figure 10(a) shows the well-known trend of increasing peak and exhaust soot values as EGR level is raised. KIVA-3V simulation suggests that the significant higher in-cylinder soot mass is due to the rise in formation rate during the pre-mix and early mixing control phases of the combustion. This increased formation rate is attributed to the less complete combustion of locally rich air-fuel mixture in reduced oxygen concentrations environment, leading to an increased proportion of fuel vapour undergoing pyrolysis to form soot precursors. The effect of EGR on the soot distribution is relatively weak. This is illustrated by the comparison shown in Figure 10(b). At the chosen crank angle position of 8.0° ATDC, the concentration within the soot cloud is higher at higher EGR levels but the size and distribution of the cloud is similar for both the low and high EGR cases.

The influence of EGR on NO concentration is shown in Figure 11(a). The engine-out NO concentration has been reduced by two-third of the level when EGR was zero. From the temporal variations, this reduction in tailpipe NO is given by the slightly delayed onset of NO production, lower rate of increase in NO concentration and a shorter production window relatively to when EGR is zero. The NO production has been seized when EGR is introduced as both charge temperature and oxygen content are lowered. As with the soot clouds, NO distributions in and around the cylinder are not affected by the EGR levels, although the increased NO concentration reflects the higher in-cylinder NO values.

4. Discussion and Conclusion

The simulations show the temporal soot and NO variations is largely set by the ratio and separation of the split main injection, whereas the influences of SOI timing and the level of EGR are generally to be seen in the scaling up or down of these variations with crank angle. Split main ratio, separation and injection timing are predicted to have the strongest influence on the transport of soot and NO in and around the chamber, with very strong interaction among these on the compounded effect of species distribution and concentration. EGR only affect the soot and NO content, with a much weaker influence on the distributions.

The effect of increasing split main ratio when the separation is small has been to increase soot mass but lower the NO concentration values. As the separation between the pulses is prolonged, the apparent influence of ratio on soot and NO is completely reversed. When closely coupled, the highest injection ratios give the higher values of soot throughout
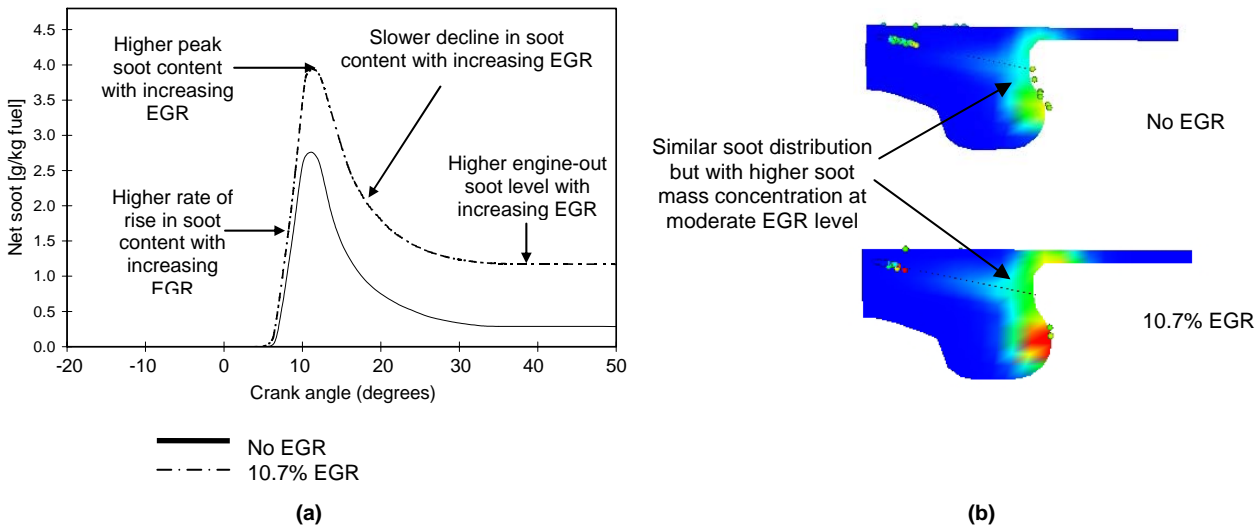

(a)

(b)

Fig 10: Effects of EGR levels under 2.0° ATDC main SOI at fixed 60/40 ratio and 0.0° separation conditions on
(a) in-cylinder net soot content,
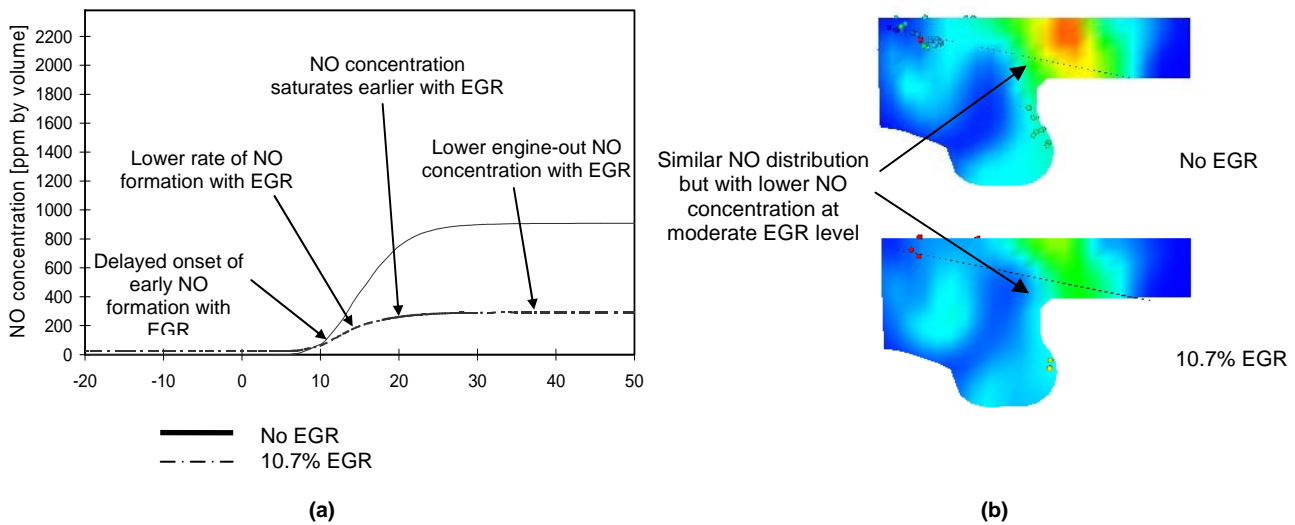(b) spatial distribution of soot at 8.0° ATDC.

(a)

(b)

Fig 11: Effects of EGR levels under 2.0° ATDC main SOI at fixed 60/40 ratio and 0.0° separation conditions on
(a) in-cylinder NO concentration,
(b) spatial distribution of NO at 20.0° ATDC.

without much influence on the spatial distribution. The primary soot cloud is not affected by the second injection, in the same manner as the total soot content. For cases with large separation, ratios are found to only influence the soot mass associated with the first injection but not its distribution. However, both the mass content and spatial location of the soot cloud due to the second injection are strongly governed by the ratio parameter. In the case of NO production, increasing the ratios when the separation is small limits the mass fraction of high temperature gas required for NO generation. The effect of ratio on NO distribution becomes more obvious as higher fraction of NO concentration is displaced into the squish region by decreasing the ratios at small separation. As the separation is increased from 0° to 20°, an increase in NO concentration is seen without any effect on its distribution for cases with higher ratios. When separations are large, the second injection comes too late in the expansion stroke to produce more high-temperature gas associated with NO production. From the observation, the fuel in the first injection is all-important in dictating the distribution and amount of NO and soot.

In all applications, SOI timing affects both the soot and NO concentrations in an opposite manner from one another. When soot mass is lowered with advanced injection, NO concentration will inevitably be raised. However, injection timing has the same effect on the distributions for both NO and soot by displacing them further into the outer combustion region as the main injection is delayed. The influence of EGR is only on the concentration and size of the NO and soot clouds, with successful NO formation control at the expense of increasing soot mass content when EGR is introduced.

There is no direct validation of predicted temporal and spatial variations of species. Although these variations are influenced by the choice of empirical coefficient values for submodels, it is possible to choose values which give predictions consistent with evidence in the literature. This approach has been followed to contain uncertainties, even if it does not eliminate them entirely. The KIVA-3V simulation study has yielded explanations to the pollutants trends and in-cylinder distribution produced by increasingly complex fuel injection strategies, in this case showing how split main ratio and separation interact at one operating condition and how the SOI timing and EGR will moderate or enhance the effect. The approach of combining CFD and test-bed studies has proven to be particularly effective to expand on the limited details of the engine-out emissions measurement.

5.   References

[1]   Ng, H.K. *The Simulation of Combustion in Diesel Engines Using KIVA-3V on a PC Platform*. Ph.D. Thesis, The University of Nottingham, 2003.

[2]   "Powertrains and the Variety of Hybrid Cars get a Heavy Airing". *Professional Engineering Magazine*, Professional Engineering Publishing, Vol. 19, 7, pp 15, 12 April 2006.

[3]   Heywood, J.B. *Internal Combustion Engine Fundamentals*. New York: McGraw-Hill, 1988.

[4]   Streets, D.G. *et al*. "An Inventory of Gaseous and Primary Aerosol Emissions in Asia in the Year 2000." *Journal of Geophysical Research*, Vol. 108, D21, 8809, 2003.

[5]   Lloyd, A.C. and Cackette, T.A. "Diesel Engines: Environmental Impact and Control." *Journal of the Air and Waste Management Association*, Vol. 51, June 2001.

[6]   Brooks T D, Pugh G J, Gambrill R, Shayler P J. "Investigating the Effects of Split Main Fuel Injection Parameters on NO_x, Soot, HC and CO Emissions from a Light Duty Diesel Engine." *Proceedings of IMechE Conference C622, Internal Combustion Engine Performance and Emissions*, London, 2005.

[7]   Ng, H.K. and Shayler, P.J. "The Installation of KIVA-3V CFD code on PCs and Performance Benchmarking for the Simulation of Combustion in Internal Combustion Engines." *Journal of the Energy Institute*, 77, pp 90-96, Dec. 2004.

[8]   O'Rourke, P.J. and Amsden, A.A. "Three-Dimensional Numerical Simulations of the UPS-292 Stratified Charge Engine." *SAE Paper 870597*, 1987.

[9]   Amsden, A.A., Butler, T.D. and O'Rourke, P.J. "The KIVA-II Computer Program for Transient Multidimensional Chemically Reactive Flows with Sprays." *SAE Paper 872072*, 1987.

[10]   Group T-3. *KIVA-3V Source Code*. New Mexico: Los Alamos National Laboratory, 1998.

[11]   Amsden A.A. *KIVA-3: A KIVA Program with Block-Structured Mesh for Complex Geometries*. Los Alamos National Laboratory, LA-12503-MS, 1993.

[12]   Varnavas, C.A. and Assanis, D.N. "The Effects of Spray, Mixing and Combustion Model Parameters on KIVA-II Predictions." *SAE Paper 911785*, 1991.

[13]   Westbrook, C.K. and Dryer, F.L. "Chemical Kinetic Modelling of Hydrocarbon Combustion." *Progress in Energy and Combustion Science*, Vol. 10, 1-57, 1984.

[14]   Amsden A.A. *KIVA-3V: A Block-Structured KIVA Program for Engines with Vertical or Canted Valves*. Los Alamos National Laboratory, LA-13313-MS, 1997.

[15]   Magnussen, B.F. and Hjertager, B.H. "On Mathematical Modelling of Turbulent Combustion with Special Emphasis on Soot Formation and Combustion." *Sixteenth Symposium (International) on Combustion*, 719-729, 1977.

[16]   Launder, B.E. and Spalding, D.B. *Computer Methods in Applied Mechanics and Engineering*, Vol. 3, 269, 1974.

[17]   O'Rourke, P.J. and Amsden, A.A. "A Particle Numerical Model for Wall Film Dynamics in Port-Injected Engines." *SAE Paper 961961*, 1996.

[18]   Amsden A.A., O'Rourke P.J. and Butler T.D. *KIVA-II – A Computer Program for Chemically Reactive Flow with Sprays*. Los Alamos National Laboratory, LA-11560-MS, 1989.

[19]   Amsden, A.A., Ramshaw, J.D., O'Rourke, P.J. and Dukowicz, J.K. *KIVA: A Computer Program for Two- and Three-Dimensional Fluid Flows with Chemical Reactions and Fuel Sprays*. Los Alamos National Laboratory, LA-10245-MS, 1985.

[20]   Han, Z. and Reitz, R.D. "Turbulence Modelling of Internal Combustion Engines Using RNG κ-ε Models." *Combustion Science and Technology*, Vol. 106, 267-295, 1995.

[21] O'Rourke, P.J. and Amsden, A.A. "The TAB Method for Numerical Calculation of Spray Droplet Break-up." *SAE Paper 872089*, 1987.

[22] Liu, A.B., Mather, D. and Reitz, R.D. "Effects of Drop Drag and Breakup on Fuel Sprays." *SAE Paper 930072*, 1993.

[23] Amsden A.A. *KIVA-3V, Release 2, Improvements to KIVA-3V*. Los Alamos National Laboratory, LA-UR-99-915, 1999.

[24] Dec, J.E. and Canaan, R.E. "PLIF Imaging of NO Formation in a DI Diesel Engine." *SAE Paper 980147*, 1998.

[25] Merryman, E.L. and Levy, A. "Nitrogen Oxide Formation in Flames: The Roles of NO_2 and Fuel Nitrogen." *Proceeding of Fifteenth International Symposium on Combustion*, 1073, The Combustion Institute, 1975.

[26] Egnell, R. "The Influence of EGR on Heat Release Rate and NO Formation in a DI Diesel Engine." *SAE Paper 2000-01-1807*, 2000.

[27] Heywood, J.B. "Pollutant Formation and Control in Spark-Ignition Engines." *Progress in Energy and Combustion Science*, Vol. 1, 135, 1976.

[28] Bowman, C.T. "Kinetics of Pollutant Formation and Destruction in Combustion." *Progress in Energy and Combustion Science*, Vol. 1, 33, 1975.

[29] Warnatz, J., Maas, U. and Dibble, R.W. *Combustion: Physical and Chemical Fundamental, Modelling and Simulation, Experiments, Pollutant Formation*. Germany: Springer-Verlag, 1996.

[30] Turns, S.R. *An Introduction to Combustion: Concepts and Applications*. US: McGraw-Hill Inc., 1996.

[31] Surovikin, V.F. "Analytical Description of the Processes of Nucleus-Forming and Growth of Particles of Carbon Black in the Thermal Decomposition of Aromatic Hydrocarbon in the Gas Phase." *Solid Fuel Chemistry*, Vol. 7, 92, 1976.

[32] Gentry, R.A., Daly, B.J. and Amsden, A.A. *KIVA-COAL: A Modified Version of the KIVA Program for Calculating the Combustion Dynamics of a Coal-water Slurry in a Diesel Engine Cylinder*. Los Alamos National Laboratory, LA-11045-MS, 1987.

[33] Roth, P. and von Gersum, S. "High Temperature Oxidation of Soot Particles by O, OH, and NO." *Turbulence and Molecular Processes in Combustion* (Takeno, T.(eds.)), Elsevier, Amsterdam, 1993.

[34] Stanmore, B.R., Brilhac, J.F. and Gilot, P. "The Oxidation of Soot: A Review of Experiments, Mechanisms and Models." *CARBON*, 39: 2247-2268, 2001.

[35] Glassman, I. *Combustion*. 3rd Edition. San Diego: Academic Press Inc., 1996.

[36] Haynes, B.S. and Wagner, H.Gg. "Soot Formation." *Progress in Energy and Combustion Science*, Vol. 7, 229, 1981.

[37] Nagle, J. and Strickland-Constable, R.F. "Oxidation of Carbon Between 1000-2000°C." *Proc. of the Fifth Conf. On Carbon*, 154. London: Pergamon Press, 1962.

[38] Park, C. and Appleton, J.P. 1973. "Shock-Tube Measurements of Soot Oxidation Rates." *Combustion Flame*, Vol. 20, 369, 1973.

[39] AVL. *AVL 415S Smoke Meter: The New Correlation Curve* [Online]. Available at: <URL: http://tec.avl.com/> [Accessed 18 February 2003], 2002.

[40] Christian, R., Knopf, F., Jaschek, A. and Schindler, W. "A New Method for the Filter Smoke Number Measurement with Improved Sensitivity." *MTZ Motortechnische Zeitschrift*, Vol. 54, 1, 1993.

[41] Stone, R. *Introduction to Internal Combustion Engine*. 3rd Edition. London: Macmillan Press Ltd., 1999.

[42] P.J. Shayler and H.K. Ng. "Simulation Studies of the Effect of Fuel Injection Pattern on NO and Soot Formation in Diesel Engines." *SAE Paper 2004-01-0116*, 2004.